HHS Public Access

Author manuscript

Cancer Prev Res (Phila). Author manuscript; available in PMC 2023 November 01.

Published in final edited form as:

Cancer Prev Res (Phila). 2023 May 01; 16(5): 247–258. doi:10.1158/1940-6207.CAPR-23-0004.

Precision cut lung slices as a preclinical model for non-small cell lung cancer chemoprevention

Kayla Sompel[1], **Alex J. Smith**[2], **Caroline Hauer**[3], **Alamelu P. Elango**[3], **Eric T. Clamby**[4], **Robert L. Keith**[3,5], **Meredith A. Tennis**[3,*]

[1]School of Medicine, University of Colorado Anschutz Medical Campus, Aurora CO

[2]Department of Molecular and Cellular Biology, Baylor College of Medicine, Houston, TX

[3]Division of Pulmonary Sciences and Critical Care Medicine, School of Medicine, University of Colorado Anschutz Medical Campus, Aurora CO

[4]Department of Anesthesiology, School of Medicine, University of Colorado Anschutz Medical Campus, Aurora CO

[5]Rocky Mountain Regional VA Medical Center, Aurora, CO

Abstract

Lung cancer chemoprevention is critical to addressing cancer burden in high-risk populations. Chemoprevention clinical trials rely on data from pre-clinical models however, *in vivo* studies have high financial, technical, and staffing requirements. Precision cut lung slices (PCLS) provide an *ex vivo* model that maintains the structure and function of native tissues. This model can be used for mechanistic investigations and drug screenings and reduces the number of animals and time required to test hypotheses compared to *in vivo* studies. We tested use of PCLS for chemoprevention studies, demonstrating recapitulation of *in vivo* models. Treatment of PCLS with the PPARγ agonizing chemoprevention agent iloprost produced similar effects on gene expression and downstream signaling as *in vivo* models. This occurred in both wildtype tissue and in Frizzled 9 knockout tissue, a transmembrane receptor required for iloprost's preventive activity. We explored new areas of iloprost mechanisms by measuring immune and inflammation markers in PCLS tissue and media, and immune cell presence with immunofluorescence. To demonstrate potential for drug screening, we treated PCLS with additional lung cancer chemoprevention agents and confirmed activity markers in culture. PCLS offers an intermediate step for chemoprevention research between *in vitro* and *in vivo* models that can facilitate drug screening prior to *in vivo*

*Corresponding Author: Meredith Tennis, University of Colorado Anschutz Medical Campus, Division of Pulmonary Sciences and Critical Care Medicine, 12700 E 19th AVE, RC2 Box C272, Aurora, CO 80045, Phone: 303-724-6073, Meredith.Tennis@cuanschutz.edu.

Author Contributions

Conceptualization: MT, AS
Methodology: KS, AS, EC
Investigation: KS, AS, AE, CH
Funding acquisition: MT
Project administration: AE, MT, RK
Supervision: MT
Writing – original draft: KS, MT
Writing – review & editing: KS, AS, EC, MT, RK

The authors declare no potential conflicts of interest.

studies and support mechanistic studies with more relevant tissue environments and functions than *in vitro* models.

Introduction

Lung cancer is the leading cause of cancer-related deaths and the second most common cancer in both men and women, with more than 120,000 deaths in the United States in 2022 and an 22% overall five-year survival rate.(1) Chemoprevention of lung cancer is a promising approach to reducing mortality and may have a larger impact than lung cancer therapy on improving outcomes for high risk populations. Chemoprevention for lung cancer is not currently available to patients, however, success of chemoprevention in other cancer types and promising agents currently in development for lung cancer chemoprevention support continued investigation.(2,3) Iloprost, a prostacyclin analog that activates peroxisome proliferator activated receptor gamma (PPARγ) signaling, is one of the most promising lung cancer chemoprevention agents in development. As a repurposed drug approved to treat pulmonary hypertension, iloprost had considerable pre-clinical evidence of preventive efficacy before moving to a phase II clinical trial, where it improved endobronchial dysplasia in former smokers.(4) Preclinical studies are critical to advancing lung cancer chemoprevention agents, as previous chemoprevention clinical trials based largely on epidemiologic data were not successful.(5) Chemoprevention agents also need extensive evidence of mechanism and response to be accepted for use in large populations. To support this for iloprost, we have investigated iloprost *in vitro* and *in vivo*, identifying potential response markers, clarifying critical pathway components, and testing delivery approaches.(6–11) We discovered that the transmembrane receptor Frizzled 9 (FZD9) is required for *in vitro* and *in vivo* preventive effects of iloprost, however, additional work is required to define this relationship and other critical aspects of iloprost as chemoprevention. Pre-clinical models support these mechanistic investigations and chemoprevention drug screening however, *in vivo* models are limited by cost and burden to animals and research staff.

Precision cut lung slices (PCLS) are produced by making slices from murine lungs and maintaining them in culture.(12) By generating multiple tissue pieces from a single mouse, PCLS increases the number of analyses that one mouse can be used for, reducing the number of animals required to address hypotheses. Manipulations to investigate mechanisms can be made in PCLS *ex vivo* in significant numbers, in contrast to *in vivo* where often genetically engineered mice or multiple treatments must be used. Conducting treatments *ex vivo* may also reduce the potential suffering of animals and stress on research staff administering complicated carcinogenesis and prevention protocols. The critical advantage of PCLS over 2D cultures or 3D organoids is that PCLS maintains native architecture, resident cell types, signaling, and responses, providing a functional heterogenous environment.(13) PCLS is used to model lung diseases such as bacterial infections, fibrosis, COPD, allergies and asthma.(14–16) Innate immunity to viral infections can be studied in PCLS, with detection of cytokines and chemokines in the media.(17) In studies of idiopathic pulmonary fibrosis, both murine and human PCLS treated with the anti-fibrotic drugs pirfenidone and nintedanib responded to the drug and PCLS provided new data on mechanisms and markers.(18)

Here, we present an *ex vivo* model using PCLS for investigation of premalignancy and chemoprevention, with discovery of new directions for research in iloprost chemoprevention.

Materials and Methods

Animals and PCLS: Frizzled 9 knockout mice (*Fzd9*$^{-/-}$) on an FVB/N (RRID:MGI:3528175) background were developed by the Regional Mouse Genetics Core Facility at National Jewish Health and the University of Colorado as previously described.(19) Wild type female FVB/N mice (eight weeks old, Charles River Laboratories) and female *Fzd9*−/− mice were housed in a pathogen-free facility in the Rocky Mountain Regional Veterans Medical Center (RMRVAMC) Veterinary Medical Unit (VMU). Wild type and *Fzd9*$^{-/-}$ mice received a lethal dose of Fatal Plus at 10–12 weeks old and lungs were harvested for PCLS. For the urethane study, mice were divided into four groups: wild type saline, wild type urethane, *Fzd9*$^{-/-}$ saline, and *Fzd9*$^{-/-}$ urethane. Mice were injected IP with 100μl of 1mg urethane/gram body weight dissolved in 0.9% saline vehicle or 100ul 0.9% saline vehicle. Mice were weighed daily for seven days after urethane injection and weekly for the remainder of the experiment. Ten weeks after urethane exposure, mice received a lethal dose of Fatal Plus and lungs were harvested for PCLS. Animal numbers for urethane exposure were based on expected lung slice/punch yield and punch number was determined by endpoint assay needs. At 14 weeks, urethane exposed FVB/N mice have an average of four visible adenomas, and we expect that at 10 weeks, animals exposed to urethane would likely have four or more hyperplasias and one visible adenoma.(8) Wild type FVB/N mice were used to generate PCLS for chemoprevention treatment experiments. All animal experiments were reviewed and approved by the RMRVAMC VMU IACUC.

To generate PCLS after mouse sacrifice, the lungs were cleared with 10mL of 1X sterile phosphate buffered saline (PBS) through the right ventricle (Fig. 1A). Immediately after, the lungs were filled through the trachea with 1mL of 1.5% low melting point agarose dissolved in sterile HEPES buffer. The whole mouse was placed on ice for 10 minutes before the lungs were extracted and placed in 1mL of 1X DMEM media with 0.1% Pen/Strep/Amphotericin B. The lobes were then sliced into 500μM slices with a vibratome at 12mM/s speed. Standardized punches were created with a 4mm biopsy punch. The punches were then washed with media three times to remove agarose, with 30-minute incubations at 37°C between each wash. Punches were cultured in 24 well plates for seven days *ex vivo* in 500μL Dulbecco's Modified Eagle Medium/Nutrient Mixture F12 (DMEM:F12) media with 0.1% fetal bovine serum and 0.1% Pen/Strep/Amphotericin B.

PCLS treatments: For the lipopolysaccharide (LPS) experiment, PCLS cultures were treated in triplicate with 10ng/ml LPS or vehicle control for 48 hours. For Iloprost experiments, PCLS cultures were treated in triplicate with 3.6μg/ml (10μM) of Iloprost (Cayman Chemical) or equal volume vehicle control (methyl acetate; 9mM final concentration) every 48 hours.(9,10) For curcumin experiments, PCLS cultures were treated in triplicate with 3.0μg /mL (8μM) or 4.5μg /mL (12μM) of curcumin (Cayman Chemical) or equal volume vehicle control (sterile water) every 24 hours.(20) For the pioglitazone experiment, PCLS cultures were treated in triplicate with 0.12μg /mL (0.34μM) or 0.18μg /mL (0.5μM) of pioglitazone (Cayman Chemical) or equal volume vehicle control (Dymethyl sulfoxide,

DMSO; Fisher Scientific) every 24 hours.(21) For the budesonide experiment, PCLS cultures were treated in triplicate with 8.7μg /ml (10μM) or 13μg g/ml (15μM) of budesonide (Cayman Chemical) or vehicle control (ethanol) every 24 hours.(22) Experiments were conducted in triplicate.

Viability assays: Metabolic activity was measured by the presto blue assay. 50μL of presto blue cell viability reagent (Fisher Scientific) was added to 500μL of media in each PCLS well. The punches were incubated at 37°C for two hours. Following incubation, 150μL was removed and placed in a clear 96 well plate in triplicate for each punch. Fluorescence was measured at 520nm on the Glomax. Analyses were conducted in triplicate statistical analysis was done by Students t-test or one-way Anova with Tukey's posthoc analysis in GraphPad Prism (RRID:SCR_002798, version 9.0.2).

qPCR: Three punches of the same experimental group were pooled into experimental triplicates, and RNA was extracted with the RNeasy Plus kit (Qiagen). qPCR Prime PCR Assays (Bio-Rad) for mouse included: E-cadherin, Vimentin, and Snai1, Cox2, IL1β, IL-6, IL-10, TNF-α, Arg1, iNos, Siglec F, 15pgdh, CyclinD1, and Prkcq. qPCR was conducted using standard protocol for SsoAdvanced SYBR Green Master Mix (Bio-Rad) on a CFX96 Touch (Bio-Rad). All gene expression data was normalized to the reference gene RPS18 and fold changes were calculated using the 2-ΔΔCt method. PCR analysis was conducted in triplicate and statistical analysis was done by Students t-test or one-way Anova with Tukey's posthoc analysis in GraphPad Prism (RRID:SCR_002798, version 9.0.2).

Peroxisome proliferator activated receptor gamma (PPARγ) response element (PPRE) luciferase assay: Media was collected from PCLS punches 24 hours after each treatment with pioglitazone or iloprost. A549 cells (RRID:CVCL_0023) were purchased from ATCC with certified authentication and negative mycoplasma testing; cells were expanded, aliquoted and cultured for a maximum of ten passages, so additional authentication and testing were not done. A549 cells were seeded at 2500 cells/well in a 96 well plate. After 24 hours, wells were transfected with 45ng PPRE (a gift from Bruce Spiegelman; RRID:Addgene_1015) and 5ng renilla control reporter vector (Promega) using TransIT-X2 transfection reagent (Mirus Bio) per the manufacturer's protocol. Mock and empty transfection controls were included. 15μl PCLS media was added to the A549 culture at 24 hours and 48 hours post transfection. Media treatments were conducted in triplicate. Luciferase activity was measured after 48 hours using the Dual-Luciferase Reporter assay kit (Promega) on a Glomax instrument (Promega). PPRE firefly activity was normalized to renilla activity and analyzed relative to untreated controls. Significance was assessed by Students t-test or one-way Anova with Tukey's posthoc analysis in GraphPad Prism.

Immunoblot: Inflammatory signaling was measured by a mouse inflammation array (RayBiotech #AAM-INF-1–8; map in Supplementary Table S1). Media was collected on day six of PCLS culture and pooled from three PCLS punches for each experimental condition. One blot per experimental group was incubated in sample media over night at 4°C, followed by incubations with 1X Biotinylated antibody cocktail and 1X horseradish peroxidase (HRP)-Streptavidin at room temperature for two hours each, per the manufacturer's protocol. The membranes were imaged with a BioRad Chemidoc Imager.

Intensities for each cytokine were averaged between the two technical replicates on each blot. The intensities for each cytokine were then compared following positive control normalization between blots, per the manufacturer's protocol.

Histology: PCLS were fixed in 1mL of 4% paraformaldehyde (PFA) at 37°C for 30 minutes. The PFA was removed and the PCLS were submerged in 1mL of 100mM glycine at 37°C for 15 minutes. The glycine was removed and the PCLS were equilibrated in 1mL of optimal cutting temperature (OCT) embedding compound (Fisher Healthcare) for 48 hours at room temperature. The PCLS were then placed in OCT medium in a base mold (Fisher Scientific), oriented in a vertical position optimal for cross sectioning, and flash frozen in liquid nitrogen. 30μM cross sections were made on a cryostat and placed in positively charged superfrost histology slides (Fisher Scientific). H&E stains were performed with a standard protocol for frozen sections.

Vectra Polaris: PCLS were fixed in 10% Formalin (Fisher Scientific) for 24 hours at room temperature. Following fixation PCLS were rinsed three times with 1X PBS. PCLS were processed and embedded into paraffin embedded blocks and sectioned onto histology slides at 4.5uM. Through our collaboration with the Human Immune Monitoring Shared Resource (HIMSR) at the University of Colorado School of Medicine we performed multispectral imaging using the Akoya Vectra Polaris instrument. This instrument allows for phenotyping, quantification, and spatial relationship analysis of tissue infiltrate in formalin-fixed paraffin-imbedded (FFPE) biopsy sections. FFPE tissue sections were stained consecutively with specific primary antibodies according to standard protocols provided by Akoya and performed routinely by the HIMSR (Antibodies, suppliers, and concentrations in Supplementary Table S2). Briefly, the slides were deparaffinized, heat treated in antigen retrieval buffer, blocked, and incubated with primary antibodies for CD3, FOXP3, CD8, B220, CD4, CD45, Vimentin, and F480, followed by HRP-conjugated secondary antibody polymer, and HRP-reactive Opal fluorescent reagents that use tyramide signal amplification (TSA) chemistry to deposit dyes on the tissue immediately surrounding each HRP molecule. Nuclei were stained with DAPI. To prevent further deposition of fluorescent dyes in subsequent staining steps, the slides were stripped in between each stain with heat treatment in antigen retrieval buffer. Whole slide scans were collected using the 10x objective and multispectral images were collected using the 20x objective with a 0.5micron resolution. The 9-color images were analyzed with inForm software V2.6 (RRID: SCR_019155) to unmix adjacent fluorochromes, subtract autofluorescence, segment the tissue, compare the frequency and location of cells, segment cellular membrane, cytoplasm, and nuclear regions, score each cellular compartment, and phenotype infiltrating immune cells according to morphology and cell marker expression.

Data Availability: The data in this study are available upon request from the corresponding author.

Results

Ex vivo PCLS recapitulates *in vivo* signaling

Treatment of lung epithelial cells and mice with iloprost leads to activation of the PPARγ response element (PPRE) and decreased EMT gene expression.(7–9) Loss of the transmembrane receptor Frizzled 9 (Fzd9) reduces downstream signaling and the preventive effects of iloprost in lung epithelial cells and in mice.(7,11) We treated wild type mouse PCLS with iloprost in culture and demonstrated maintenance of tissue structure by H&E (Fig. 1B) compared to the vehicle control at day one and day seven, and maintenance of viability over seven days (Fig. 1C) by presto blue assay. We confirmed that at this standard *in vitro* dose for seven days, iloprost does not reduce viability or affect tissue integrity. To measure gene expression and PPARγ activity, we generated PCLS for wild type and *Fzd9* knockout mice ($Fzd9^{-/-}$). Consistent with prior *in vivo* results, a dual-luciferase PPRE assay at culture day six indicated significantly increased PPARγ activity with iloprost treatment in wildtype PCLS and no effect of iloprost on PPRE in $Fzd9^{-/-}$ PCLS (Fig. 1D). We also found that iloprost significantly increased *E-cadherin* expression by qPCR in wild type PCLS but had no effect on *E-cadherin* levels in $Fzd9^{-/-}$ PCLS (Fig. 1E).

To further validate and expand PCLS as a lung cancer chemoprevention model, we tested effects of iloprost in PCLS generated from mice exposed *in vivo* to urethane, which are expected to have premalignant hyperplasia and microadenomas. Previous studies demonstrated increased PPRE activity in mouse serum after iloprost treatment in the urethane model and found changes in gene expression.(7,8) FVB/N mice were exposed to urethane or vehicle control *in vivo* for ten weeks. Mice were harvested and PCLS containing premalignant lesions were generated and exposed to Iloprost or vehicle control for seven days of culture. Presto blue assay confirmed that PCLS treated with iloprost after *in vivo* urethane were viable through day seven (Fig. 2A). PPRE activity induced by culture media increased with iloprost treatment in PCLS from control and urethane mice at culture day three (Fig. 2B). Iloprost treatment reduces expression of mesenchymal genes that are induced by urethane, so we measured this in PCLS after iloprost.(7,9,10) Gene expression analysis by qPCR detected a significant decrease in *Vim* and *Snai1* with iloprost treatment in control and urethane tissues, as well as a near significant decrease in *Cox2* expression (Fig. 2C). A non-significant increase in E-cadherin expression was detected in urethane exposed mice treated with iloprost in PCLS (Fig. 2C). This was reduced compared to wild type PCLS with iloprost treatment (Fig. 1E), potentially due to age or exposure differences. While *in vivo* models demonstrate a significant difference in E-cadherin expression between urethane and urethane/iloprost tissues, variability in the PCLS samples may have reduced observable differences.

Immune and inflammatory responses in PCLS

We have investigated signaling pathways and lesion generation following iloprost treatment and FZD9 loss *in vitro* and *in vivo*, but little is known about immune or inflammatory responses in these conditions. A PCLS model could provide a new approach to identifying mechanisms of chemoprevention drug activity. To demonstrate active inflammatory responses in PCLS, we measured the effects of lipopolysaccharide (LPS) in wildtype and

Fzd9$^{-/-}$ PCLS by treating with LPS for ten days (Fig. 3A). Markers of LPS exposure increased with in wild type PCLS and in some cases had different levels in *Fzd9*$^{-/-}$ PCLS, suggesting that loss of Fzd9 may impact inflammatory response. Changes in cytokine expression in wildtype and *Fzd9*$^{-/-}$ PCLS were measured by qPCR (Fig. 3B). We detected increased expression of *IL6* with iloprost but no change in *Fzd9*$^{-/-}$ PCLS. *IL10* expression decreased with iloprost in wildtype mice but no change was detected in *Fzd9*$^{-/-}$ PCLS. Changes in macrophages are associated with premalignant lesions and iloprost treatment, so we wanted to measure changes or presence of macrophages in our PCLS.(23,24) qPCR detected significant increases in expression of *SiglecF* (a protein expressed by alveolar macrophages) and iNos (an IFNγ-inducible effector molecule expressed by macrophages) in Iloprost treated wildtype or Fzd9$^{-/-}$ PCLS (Figure 3C). Expression of *Arg1,* a gene expressed by alternatively activated M2 macrophages, was significantly higher with iloprost treatment in *Fzd9*$^{-/-}$ mice compared to wild type mice (Fig. 3C). Media from three PCLS samples was pooled for cytokine analysis by dot blot array in wildtype and *Fzd9*$^{-/-}$ PCLS treated with iloprost. Cytokine analysis identified potential changes related to iloprost or loss of *Fzd9* compared to a wildtype control (Fig. 3D, Supplementary Figure S1). In both tissue types, Iloprost increased CCL1, CXCL1, IL6, and M-CSF and decreased TNFRII compared to control. Loss of FZD9 led to elevated Eotaxin-2 and TNFRII and lower IL12 p70 and MIP-1γ. The combination of FZD9 loss and iloprost resulted in higher IL1a, CXCL1, Eotaxin-2, and M-CSF and lower CCL2 compared to other conditions.

In similar analysis of *in vivo* urethane exposed, *ex vivo* iloprost treated PCLS, iloprost decreased expression of *TNFα* in control and urethane exposed tissue (Fig. 4A). Iloprost increased expression of *IL6* in saline tissue but had a diminished effect in urethane tissue (Fig. 4A). A previous *in vivo* study found increased *IL1β* expression with urethane that was significantly decreased by iloprost.(8) Here, urethane tissue had slightly elevated *IL1β* expression that was also significantly decreased by iloprost (Fig. 4A). Iloprost significantly decreased *IL10* expression in saline tissue but did not significantly alter elevated *IL10* in urethane tissues (Fig. 4A). Analysis of macrophage markers found significantly increased expression of *iNos* and *SiglecF* with iloprost in saline tissues but a trend to the opposite in urethane tissues with iloprost (Fig. 4B). Though not significant, *Arg1* expression was elevated with urethane and iloprost treatment after urethane decreased this expression (Fig. 4B). We conducted a dot blot analysis of cytokine expression in these PCLS and found that compared to the saline-vehicle control, iloprost increased CXCL1, LIX, and CCL2, and iloprost caused a large increase in IL6 in both saline and urethane PCLS (Fig. 4C, Supplementary Figure S2). Urethane exposure led to decreased LIX and increased Eotaxin-2 (Fig. 4C). The effect on Eotaxin-2 was reversed by iloprost but the effect on LIX was not. Urethane exposure also prevented iloprost induced changes in CXCL1 and CCL2. A slight decrease in TNFRII caused by iloprost in saline tissues was lower with iloprost in urethane tissues.

Immune cells in PCLS

A key advantage of the PCLS model is inclusion of most resident cell types in the sliced tissue, however, the stability of different cell types in PCLS likely varies. We conducted initial measurements of immune cell presence to support use of this model

for chemoprevention agents related to immune or inflammatory modulation. Immune cell presence was determined by immunofluorescence (Vectra Polaris; Marker combinations in Supplementary Table S3.) in wildtype and *Fzd9*$^{-/-}$ PCLS following culture day seven with or without iloprost (Representative images in Supplementary Figure S3). CD45+ cells were present in all conditions. *Fzd9*$^{-/-}$ PCLS displayed a higher percent of CD45+ out of total cells and iloprost had little effect on this percent in *Fzd9*$^{-/-}$ tissue (Fig. 5A). Macrophages, defined by F4/80 expression, were the most abundant immune cell type based on cell density, with a slightly higher frequency in *Fzd9−/−* PCLS (Fig. 5B, Supplementary Figure S4). T cells were the next most abundant cells, with a dominant CD4+ T cell contribution (Fig. 5B). Minimal populations of B-cells and CD8+ T cells were detected in some groups and single or no regulatory T cells (Tregs) or neutrophils were detected (Fig. 5B). Figure 5C shows the percent of CD45+ subtypes in each type of PCLS, with macrophages dominating in all PCLS but even more so in *Fzd9*$^{-/-}$ PCLS. This was complemented by a decreased proportion of T cells in *Fzd9*$^{-/-}$ PCLS. Vimentin was included in the staining panel, identifying the presence of other cell types and supporting validation of structural integrity of the PCLS (Representative images in Supplementary Figure S5).

Activity of chemoprevention agents in PCLS

A potentially valuable application of the PCLS model is to conduct high throughput screening of new chemoprevention agents prior to initiating *in vivo* studies, narrowing the field of agents, and reducing the cost and burden of animal studies. Iloprost is an agent with extensive pre-clinical evidence of preventive activity and a successful clinical trial, and its effects are recapitulated in PCLS. We chose three additional chemoprevention agents with evidence of prevention in pre-clinical studies to test in PCLS: pioglitazone, curcumin, and budesonide. (25–28) *Ex vivo* doses were determined from previous *in vitro* or *in vivo* studies.(20–22,29–31) Presto blue viability assay confirmed that pioglitazone did not exhibit significant toxicity *ex vivo* (Fig. 6A). Activation of PPARγ by pioglitazone was confirmed in PCLS media over ten days of culture (Fig. 6B). mRNA indicators of PPARγ signaling, *Cox2* and *15pgdh*, were detected by qPCR (Fig. 6C). These responses mimic *in vivo* signaling.(25,32) In previous studies, curcumin decreased expression of *IL6*, *Cyclin D1*, and *TNFα*. (33–36) PCLS treated with curcumin *ex vivo* did not have increased toxicity (Fig. 6D) and exhibited significantly lower mRNA levels of *IL6*, *CyclinD1*, and *TNFα* than those treated with the vehicle control (Fig. 6E). Budesonide decreases *Prkcq* expression *in vivo*.(22) We found that PCLS treated with budesonide did not have increased toxicity (Fig. 6F) and had significantly decreased *Prkcq* mRNA expression (Fig. 6G)

Discussion

Despite the strong interest PCLS as a preclinical model, its use in lung cancer is limited. To our knowledge, PCLS has been used in one study to make tumor slice explants from mice and humans to study targeted therapy and in a study for tumor slice optimization. (37,38) Additional exploration of this potentially valuable tool is needed to expand its use in lung cancer research. We began by confirming established responses in PCLS, based on our previous *in vivo* studies. We have conducted extensive studies on iloprost lung cancer chemoprevention, the urethane chemical carcinogenesis model, and the role of FZD9 in lung

cancer and iloprost's preventive activity, and so we selected these conditions to explore in the PCLS model. We found that PCLS recapitulated signaling in response to *ex vivo* iloprost and maintained responses observed in *Fzd9*$^{-/-}$ tissues *in vivo*. Viability of *in vivo* urethane exposed PCLS was also maintained for seven days in culture and *in vivo* gene expression and signaling was recapitulated ex vivo. These results suggests that PCLS from genetically engineered or *in vivo* carcinogen exposed mice can be maintained in culture and further manipulated to address hypotheses. This provides opportunities to conduct mechanistic studies of chemical carcinogenesis and chemoprevention with high numbers of replicates or targets but without large, burdensome animal studies. The PCLS model requires additional validation for *in vivo* progressive disease stages, as we only validated tissue with ten weeks of urethane exposure and other exposure time points may respond differently to PCLS culture.

Precision cut lung slices have been used to investigate pulmonary immune responses in a variety of contexts, including after infection, with immunomodulatory therapy, after smoke exposure, and during airway remodeling. (15,17) Little is known about effects of FZD9 or iloprost on immune or inflammatory responses in lung cancer, but as the role of the microenvironment in development of lung premalignant lesions becomes more apparent, we expect that since iloprost reduces the presence of premalignant lesions, it likely impacts components of the microenvironment.(39,40) Iloprost increased IL6 mRNA expression, which was blocked by loss of FZD9, and IL10 was decreased in *Fzd9*$^{-/-}$ PCLS compared to wildtype PCLS, regardless of iloprost treatment. Characterization of cytokines by dot blot in wildtype PCLS identified protein level effects of iloprost, such as increased CXCL1, IL6, and M-CSF. At the cytokine level, however, iloprost seemed to increase IL6 nearly equally in Fzd9−/−, which may indicate that iloprost has some effects outside of FZD9 and that these effects may not be critical for chemoprevention. This is also suggested by variation in IL6 measurements from iloprost treated urethane PCLS. The highest M-CSF or Eotaxin-2 levels were observed with iloprost treatment in *Fzd9*$^{-/-}$ mice, suggesting that some effects of FZD9 loss may be exacerbated by iloprost. We observed this phenomenon in a previous *in vivo* study, where iloprost administered to *Fzd9*$^{-/-}$ mice exacerbated some pro-cancer changes from FZD9 loss and had little protective effect.(7) In our *in vivo* urethane exposure PCLS study, *ex vivo* iloprost affected some targets in saline PCLS that were not affected with iloprost treatment in urethane PCLS, suggesting that these targets may not be critical to iloprost's preventive effects in the urethane model. IL1β decrease induced by iloprost in urethane but not saline PCLS points to IL1β as a potential target of iloprost in the reversal of pro-tumor signaling. While immune and inflammatory changes may result from damage during generation of PCLS, these generally stabilize after 24–48 hours of culture, so we expect that with seven days of culture we are observing effects of manipulations in culture.(41) Immune cells have been detected up to PCLS culture day 14, including dendritic cells, T cells, and macrophages.(42–44) Immunofluorescence in our PCLS detected markers of T cells, macrophages, and B cells, depending on conditions. Presence of different types of macrophages and CD4+ T cells characterizes regressive or progressive premalignant squamous lung lesions and there is evidence for both immune activation and suppression during early stages of lung cancer. (40,45) Depletion of macrophages reduces tumor number in A/J mice in the urethane model

of lung cancer but regressive dysplasias have more macrophages than persistent dysplasias, suggesting a varied role for macrophages depending on the stage of lesion development.(24,39) Iloprost increased the presence of macrophages in a urethane mouse model.(23) The most prominent cell type in our PCLS was macrophages, with higher frequency in *Fzd9*$^{-/-}$ PCLS compared to wild type. *Fzd9*$^{-/-}$ PCLS also had a higher frequency of CD45+ hematopoietic cells, suggesting potentially enhanced immune cell infiltration with FZD9 loss. Changes in macrophage expressed genes with iloprost treatment suggest altered activity of resident macrophages or effects on resident immune cells in the absence of new cell recruitment into the lung.(46) While we could not measure immune cell recruitment in this PCLS model, we demonstrated that resident immune cells may play an important role in chemoprevention models and can be characterized in PCLS. New populations of native or manipulated immune cells, as well as the addition of exogenous cytokines or neutralizing antibodies, could be added to PCLS culture to explore additional hypotheses.

PCLS is particularly relevant for chemoprevention drug screening, where sifting through numerous candidate drugs could be streamlined by pretesting in PCLS prior to full *in vivo* studies. However, this relies on functioning systems in PCLS tissue. We demonstrated activity of the well-studied chemoprevention agent iloprost in PCLS and activity of emerging agents curcumin, pioglitazone, and budesonide. (4,8,25–27,47–49) While cells remained over 50% viable at the doses used for these agents, additional optimization might improve viability before further investigations with these drugs. These observations in PCLS suggest that chemoprevention agents may be active *ex vivo* but that multiple assessments of activity should be considered. This could include incorporating knowledge of premalignant lesion activity or other characteristics outside of drug specific mechanisms, such as reversal of a dysplasia persistence profile or alterations in immune cell profiles.(39,40) PCLS could also be used to explore mechanisms of potential agents, test mechanisms suggested by clinical trial data, or investigate new markers of response. Screening of chemoprevention drugs with *ex vivo* models, such as PCLS, organoids, or air liquid interface cultures, may identify agents that are effective *ex vivo* but not *in vivo*. The opposite could also be true, where *ex vivo* models may exclude agents that are not effective *ex vivo* but would effective be *in vivo*. However, agents are routinely tested *in vitro* and moved to *in vivo* studies with the same risks. *Ex vivo* models will help to identify agents that are less likely to be effective *in vivo* and focus efforts on those more likely to have robust responses, reducing the time and cost of *in vivo* agent testing. Agent metabolism may be compromised, as the full complement of metabolizing enzymes may not be present in PCLS. For agents that are not active in PCLS, substitution with available metabolites or investigation of enzyme presence could determine next steps with the agent. Ideally, characterization of PCLS metabolic capacity can be done prior to agent screening to avoid potential inactivity.

While our results suggest that PCLS is useful as a model of chemoprevention, this study was focused on proof-of-principle experiments. Results from immune and inflammation analyses demonstrate that these factors can be measured in our PCLS model and may generate related hypotheses, but any conclusions in these areas will require additional studies. We did not extend our work to advanced techniques, but PCLS can be manipulated with viral transduction and adoptive cell transfer, and be used for numerous endpoint assays, including sequencing, staining, flow cytometry, and live cell imaging.(17,43,50,51) We cultured our

PCLS for seven to ten days to detect signaling changes. Others have cultured viable PCLS to three or more weeks, however, after around 15 days PCLS tend to have reduced integrity and function.(13,41) PCLS could potentially be used to study premalignant lesions or tumors but a longer culture duration will be needed to explore endpoints beyond signaling, such as changes in lesion presence, size, or proliferation. A promising recent study embedded PCLS in a bioengineered hydrogel, extending culture to more than 21 days, a time frame which could provide more opportunity to study premalignant lung lesions.(52) Our PCLS models recapitulated signaling from *in vivo* models and demonstrated capacity to detect immune and inflammatory changes, suggesting that PCLS is a viable model for *ex vivo* lung cancer chemoprevention studies. This model could decrease the burden of chemoprevention studies on animals and staff and offer a system for high throughput screening of new chemoprevention agents. The need for lung cancer chemoprevention in high-risk populations is significant and this work could address that need by substantially accelerating the pace of lung cancer chemoprevention research.

Supplementary Material

Refer to Web version on PubMed Central for supplementary material.

Acknowledgements

The authors acknowledge Dr. Lori Nield for guidance and training in mouse studies. This work was supported by the National Cancer Institute (R01CA214531) (M.A. Tennis), an NIH CURE Diversity Supplement (R01CA214531-04S1) (A.J. Smith), the Regional Mouse Genetics Core Facility (National Jewish Health and the University of Colorado Anschutz Medical Campus), the Human Immune Monitoring and Cell Technologies shared resources funded by the National Cancer Institute through The University of Colorado Cancer Center Support Grant (P30CA046934).

References

1. Siegel RL, Miller KD, Wagle NS, Jemal A. Cancer statistics, 2023. CA Cancer J Clin 2023;73(1):17–48 doi 10.3322/caac.21763. [PubMed: 36633525]
2. Bozzuto LM. Breast cancer risk reduction: who, why, and what? Best Pract Res Clin Obstet Gynaecol 2022;83:36–45 doi 10.1016/j.bpobgyn.2021.11.012. [PubMed: 34991977]
3. Perez M, Abisaad JA, Rojas KD, Marchetti MA, Jaimes N. Skin cancer: Primary, secondary, and tertiary prevention. Part I. J Am Acad Dermatol 2022;87(2):255–68 doi 10.1016/j.jaad.2021.12.066. [PubMed: 35176397]
4. Keith RL, Blatchford PJ, Kittelson J, Minna JD, Kelly K, Massion PP, et al. Oral iloprost improves endobronchial dysplasia in former smokers. Cancer Prev Res (Phila) 2011;4(6):793–802 doi 10.1158/1940-6207.CAPR-11-0057. [PubMed: 21636546]
5. New M, Keith R. Early Detection and Chemoprevention of Lung Cancer. F1000Res 2018;7:61 doi 10.12688/f1000research.12433.1. [PubMed: 29375824]
6. Smith AJ, Do P, Sompel K, Elango A, Tennis MA. miR-520a-5p regulates Frizzled 9 expression and mediates effects of cigarette smoke and iloprost chemoprevention. Sci Rep 2022;12(1):2388 doi 10.1038/s41598-022-06292-7. [PubMed: 35149732]
7. Sompel K, Dwyer-Nield LD, Smith AJ, Elango A, Backos DS, Zhang B, et al. Iloprost requires the Frizzled-9 receptor to prevent lung cancer. iScience 2022;25(6):104442 doi 10.1016/j.isci.2022.104442. [PubMed: 35707728]
8. Tennis MA, Smith AJ, Dwyer-Nield LD, Keith RL. Intranasal Iloprost Prevents Tumors in a Murine Lung Carcinogenesis Model. Cancer Prev Res (Phila) 2022;15(1):11–6 doi 10.1158/1940-6207.CAPR-21-0086. [PubMed: 34556494]

9. New ML, White CM, McGonigle P, McArthur DG, Dwyer-Nield LD, Merrick DT, et al. Prostacyclin and EMT pathway markers for monitoring response to lung cancer chemoprevention. Cancer Prev Res (Phila) 2018:643–54 doi 10.1158/1940-6207.CAPR-18-0052. [PubMed: 30045935]
10. Tennis MA, New ML, McArthur DG, Merrick DT, Dwyer-Nield LD, Keith RL. Prostacyclin reverses the cigarette smoke-induced decrease in pulmonary Frizzled 9 expression through miR-31. Sci Rep 2016;6:28519 doi 10.1038/srep28519. [PubMed: 27339092]
11. Tennis MA, Van Scoyk M, Heasley LE, Vandervest K, Weiser-Evans M, Freeman S, et al. Prostacyclin inhibits non-small cell lung cancer growth by a frizzled 9-dependent pathway that is blocked by secreted frizzled-related protein 1. Neoplasia 2010;12(3):244–53. [PubMed: 20234818]
12. Fisher RL, Smith MS, Hasal SJ, Hasal KS, Gandolfi AJ, Brendel K. The use of human lung slices in toxicology. Hum Exp Toxicol 1994;13(7):466–71 doi 10.1177/096032719401300703. [PubMed: 7917502]
13. Alsafadi HN, Uhl FE, Pineda RH, Bailey KE, Rojas M, Wagner DE, et al. Applications and Approaches for Three-Dimensional Precision-Cut Lung Slices. Disease Modeling and Drug Discovery. Am J Respir Cell Mol Biol 2020;62(6):681–91 doi 10.1165/rcmb.2019-0276TR. [PubMed: 31991090]
14. Wronski S, Beinke S, Obernolte H, Belyaev NN, Saunders KA, Lennon MG, et al. Rhinovirus-induced Human Lung Tissue Responses Mimic Chronic Obstructive Pulmonary Disease and Asthma Gene Signatures. Am J Respir Cell Mol Biol 2021;65(5):544–54 doi 10.1165/rcmb.2020-0337OC. [PubMed: 34181859]
15. Liu G, Saren L, Douglasson H, Zhou XH, Aberg PM, Ollerstam A, et al. Precision cut lung slices: an ex vivo model for assessing the impact of immunomodulatory therapeutics on lung immune responses. Arch Toxicol 2021;95(8):2871–7 doi 10.1007/s00204-021-03096-y. [PubMed: 34191076]
16. Meineke R, Stelz S, Busch M, Werlein C, Kuhnel M, Jonigk D, et al. FDA-Approved Inhibitors of RTK/Raf Signaling Potently Impair Multiple Steps of In Vitro and Ex Vivo Influenza A Virus Infections. Viruses 2022;14(9) doi 10.3390/v14092058.
17. Michalaki C, Dean C, Johansson C. The Use of Precision-Cut Lung Slices for Studying Innate Immunity to Viral Infections. Curr Protoc 2022;2(8):e505 doi 10.1002/cpz1.505. [PubMed: 35938685]
18. Lehmann M, Buhl L, Alsafadi HN, Klee S, Hermann S, Mutze K, et al. Differential effects of Nintedanib and Pirfenidone on lung alveolar epithelial cell function in ex vivo murine and human lung tissue cultures of pulmonary fibrosis. Respir Res 2018;19(1):175 doi 10.1186/s12931-018-0876-y. [PubMed: 30219058]
19. Sompel K, Dwyer-Nield LD, Smith AJ, Elango AP, Vanderlinden LA, Kopf K, et al. Loss of Frizzled 9 in Lung Cells Alters Epithelial Phenotype and Promotes Premalignant Lesion Development. Front Oncol 2022;12:815737 doi 10.3389/fonc.2022.815737. [PubMed: 35924166]
20. Fu H, Wang C, Yang D, Wei Z, Xu J, Hu Z, et al. Curcumin regulates proliferation, autophagy, and apoptosis in gastric cancer cells by affecting PI3K and P53 signaling. J Cell Physiol 2018;233(6):4634–42 doi 10.1002/jcp.26190. [PubMed: 28926094]
21. Hazra S, Batra RK, Tai HH, Sharma S, Cui X, Dubinett SM. Pioglitazone and rosiglitazone decrease prostaglandin E2 in non-small-cell lung cancer cells by up-regulating 15-hydroxyprostaglandin dehydrogenase. Mol Pharmacol 2007;71(6):1715–20 doi 10.1124/mol.106.033357. [PubMed: 17412838]
22. Yao R, Wang Y, Lemon WJ, Lubet RA, You M. Budesonide exerts its chemopreventive efficacy during mouse lung tumorigenesis by modulating gene expressions. Oncogene 2004;23(46):7746–52 doi 10.1038/sj.onc.1207985. [PubMed: 15361829]
23. Nemenoff R, Meyer AM, Hudish TM, Mozer AB, Snee A, Narumiya S, et al. Prostacyclin prevents murine lung cancer independent of the membrane receptor by activation of peroxisomal proliferator--activated receptor gamma. Cancer Prev Res (Phila) 2008;1(5):349–56 doi 10.1158/1940-6207.CAPR-08-0145. [PubMed: 19138979]

24. Fritz JM, Tennis MA, Orlicky DJ, Lin H, Ju C, Redente EF, et al. Depletion of tumor-associated macrophages slows the growth of chemically induced mouse lung adenocarcinomas. Front Immunol 2014;5:587 doi 10.3389/fimmu.2014.00587. [PubMed: 25505466]
25. Dwyer-Nield LD, McArthur DG, Hudish TM, Hudish LI, Mirita C, Sompel K, et al. PPARgamma agonism inhibits progression of premalignant lesions in a murine lung squamous cell carcinoma model. Int J Cancer 2022:2195–205 doi 10.1002/ijc.34210. [PubMed: 35830207]
26. Vijayakurup V, Thulasidasan AT, Shankar GM, Retnakumari AP, Nandan CD, Somaraj J, et al. Chitosan Encapsulation Enhances the Bioavailability and Tissue Retention of Curcumin and Improves its Efficacy in Preventing B[a]P-induced Lung Carcinogenesis. Cancer Prev Res (Phila) 2019;12(4):225–36 doi 10.1158/1940-6207.CAPR-18-0437. [PubMed: 30760502]
27. Seabloom DE, Galbraith AR, Haynes AM, Antonides JD, Wuertz BR, Miller WA, et al. Fixed-Dose Combinations of Pioglitazone and Metformin for Lung Cancer Prevention. Cancer Prev Res (Phila) 2017;10(2):116–23 doi 10.1158/1940-6207.CAPR-16-0232. [PubMed: 28052934]
28. Fu H, Zhang J, Pan J, Zhang Q, Lu Y, Wen W, et al. Chemoprevention of lung carcinogenesis by the combination of aerosolized budesonide and oral pioglitazone in A/J mice. Mol Carcinog 2011;50(12):913–21 doi 10.1002/mc.20751. [PubMed: 21374736]
29. Ciaramella V, Sasso FC, Di Liello R, Corte CMD, Barra G, Viscardi G, et al. Activity and molecular targets of pioglitazone via blockade of proliferation, invasiveness and bioenergetics in human NSCLC. J Exp Clin Cancer Res 2019;38(1):178 doi 10.1186/s13046-019-1176-1. [PubMed: 31027492]
30. Zhou QM, Wang XF, Liu XJ, Zhang H, Lu YY, Su SB. Curcumin enhanced antiproliferative effect of mitomycin C in human breast cancer MCF-7 cells in vitro and in vivo. Acta Pharmacol Sin 2011;32(11):1402–10 doi 10.1038/aps.2011.97. [PubMed: 21986579]
31. Leigh R, Mostafa MM, King EM, Rider CF, Shah S, Dumonceaux C, et al. An inhaled dose of budesonide induces genes involved in transcription and signaling in the human airways: enhancement of anti- and proinflammatory effector genes. Pharmacol Res Perspect 2016;4(4):e00243 doi 10.1002/prp2.243. [PubMed: 28116096]
32. El-Jamal N, Dubuquoy L, Auwerx J, Bertin B, Desreumaux P. In vivo imaging reveals selective PPAR activity in the skin of peroxisome proliferator-activated receptor responsive element-luciferase reporter mice. Exp Dermatol 2013;22(2):137–40 doi 10.1111/exd.12082. [PubMed: 23362873]
33. Derosa G, Maffioli P, Simental-Mendia LE, Bo S, Sahebkar A. Effect of curcumin on circulating interleukin-6 concentrations: A systematic review and meta-analysis of randomized controlled trials. Pharmacol Res 2016;111:394–404 doi 10.1016/j.phrs.2016.07.004. [PubMed: 27392742]
34. Mukhopadhyay A, Banerjee S, Stafford LJ, Xia C, Liu M, Aggarwal BB. Curcumin-induced suppression of cell proliferation correlates with down-regulation of cyclin D1 expression and CDK4-mediated retinoblastoma protein phosphorylation. Oncogene 2002;21(57):8852–61 doi 10.1038/sj.onc.1206048. [PubMed: 12483537]
35. Sahebkar A, Cicero AFG, Simental-Mendia LE, Aggarwal BB, Gupta SC. Curcumin downregulates human tumor necrosis factor-alpha levels: A systematic review and meta-analysis ofrandomized controlled trials. Pharmacol Res 2016;107:234–42 doi 10.1016/j.phrs.2016.03.026. [PubMed: 27025786]
36. Yang Q, Wu S, Mao X, Wang W, Tai H. Inhibition effect of curcumin on TNF-alpha and MMP-13 expression induced by advanced glycation end products in chondrocytes. Pharmacology 2013;91(1–2):77–85 doi 10.1159/000345345. [PubMed: 23183190]
37. Narhi K, Nagaraj AS, Parri E, Turkki R, van Duijn PW, Hemmes A, et al. Spatial aspects of oncogenic signalling determine the response to combination therapy in slice explants from Kras-driven lung tumours. J Pathol 2018;245(1):101–13 doi 10.1002/path.5059. [PubMed: 29443392]
38. Nagaraj AS, Bao J, Hemmes A, Machado M, Narhi K, Verschuren EW. Establishment and Analysis of Tumor Slice Explants As a Prerequisite for Diagnostic Testing. J Vis Exp 2018(141) doi 10.3791/58569.
39. Merrick DT, Edwards MG, Franklin WA, Sugita M, Keith RL, Miller YE, et al. Altered cell-cycle control, inflammation and adhesion in high-risk persistent bronchial dysplasia. Cancer Res 2018:4971–83 doi 10.1158/0008-5472.CAN-17-3822. [PubMed: 29997230]

40. Beane JE, Mazzilli SA, Campbell JD, Duclos G, Krysan K, Moy C, et al. Molecular subtyping reveals immune alterations associated with progression of bronchial premalignant lesions. Nat Commun 2019;10(1):1856 doi 10.1038/s41467-019-09834-2. [PubMed: 31015447]
41. Nussbaum SM, Krabbe J, Boll S, Babendreyer A, Martin C. Functional changes in long-term incubated rat precision-cut lung slices. Respir Res 2022;23(1):261 doi 10.1186/s12931-022-02169-5. [PubMed: 36127699]
42. Khan MM, Poeckel D, Halavatyi A, Zukowska-Kasprzyk J, Stein F, Vappiani J, et al. An integrated multiomic and quantitative label-free microscopy-based approach to study pro-fibrotic signalling in ex vivo human precision-cut lung slices. Eur Respir J 2021;58(1) doi 10.1183/13993003.00221-2020.
43. Lyons-Cohen MR, Thomas SY, Cook DN, Nakano H. Precision-cut Mouse Lung Slices to Visualize Live Pulmonary Dendritic Cells. J Vis Exp 2017(122) doi 10.3791/55465.
44. Carranza-Rosales P, Carranza-Torres IE, Guzman-Delgado NE, Lozano-Garza G, Villarreal-Trevino L, Molina-Torres C, et al. Modeling tuberculosis pathogenesis through ex vivo lung tissue infection. Tuberculosis (Edinb) 2017;107:126–32 doi 10.1016/j.tube.2017.09.002. [PubMed: 29050759]
45. Mascaux C, Angelova M, Vasaturo A, Beane J, Hijazi K, Anthoine G, et al. Immune evasion before tumour invasion in early lung squamous carcinogenesis. Nature 2019;571(7766):570–5 doi 10.1038/s41586-019-1330-0. [PubMed: 31243362]
46. Pfirschke C, Engblom C, Gungabeesoon J, Lin Y, Rickelt S, Zilionis R, et al. Tumor-Promoting Ly-6G(+) SiglecF(high) Cells Are Mature and Long-Lived Neutrophils. Cell Rep 2020;32(12):108164 doi 10.1016/j.celrep.2020.108164. [PubMed: 32966785]
47. Liang Z, Wu R, Xie W, Zhu M, Xie C, Li X, et al. Curcumin reverses tobacco smokeinduced epithelialmesenchymal transition by suppressing the MAPK pathway in the lungs of mice. Mol Med Rep 2018;17(1):2019–25 doi 10.3892/mmr.2017.8028. [PubMed: 29138815]
48. Galbraith AR, Seabloom DE, Wuertz BR, Antonides JD, Steele VE, Wattenberg LW, et al. Chemoprevention of Lung Carcinogenesis by Dietary Nicotinamide and Inhaled Budesonide. Cancer Prev Res (Phila) 2019;12(2):69–78 doi 10.1158/1940-6207.CAPR-17-0402. [PubMed: 30606719]
49. Veronesi G, Lazzeroni M, Szabo E, Brown PH, DeCensi A, Guerrieri-Gonzaga A, et al. Long-term effects of inhaled budesonide on screening-detected lung nodules. Ann Oncol 2015;26(5):1025–30 doi 10.1093/annonc/mdv064. [PubMed: 25672894]
50. Rosales Gerpe MC, van Vloten JP, Santry LA, de Jong J, Mould RC, Pelin A, et al. Use of Precision-Cut Lung Slices as an Ex Vivo Tool for Evaluating Viruses and Viral Vectors for Gene and Oncolytic Therapy. Mol Ther Methods Clin Dev 2018;10:245–56 doi 10.1016/j.omtm.2018.07.010. [PubMed: 30112421]
51. Stegmayr J, Alsafadi HN, Langwinski W, Niroomand A, Lindstedt S, Leigh ND, et al. Isolation of high-yield and -quality RNA from human precision-cut lung slices for RNA-sequencing and computational integration with larger patient cohorts. Am J Physiol Lung Cell Mol Physiol 2021;320(2):L232–L40 doi 10.1152/ajplung.00401.2020. [PubMed: 33112185]
52. Bailey KE, Pino C, Lennon ML, Lyons A, Jacot JG, Lammers SR, et al. Embedding of Precision-Cut Lung Slices in Engineered Hydrogel Biomaterials Supports Extended ex vivo Culture. Am J Respir Cell Mol Biol 2019:14–22 doi 10.1165/rcmb.2019-0232MA.

Prevention Relevance

Precision cut lung slices could be a new model for premalignancy and chemoprevention research, and this work evaluates the model with tissue from prevention relevant genetic and carcinogen exposed *in vivo* mouse models, in addition to evaluating chemoprevention agents.

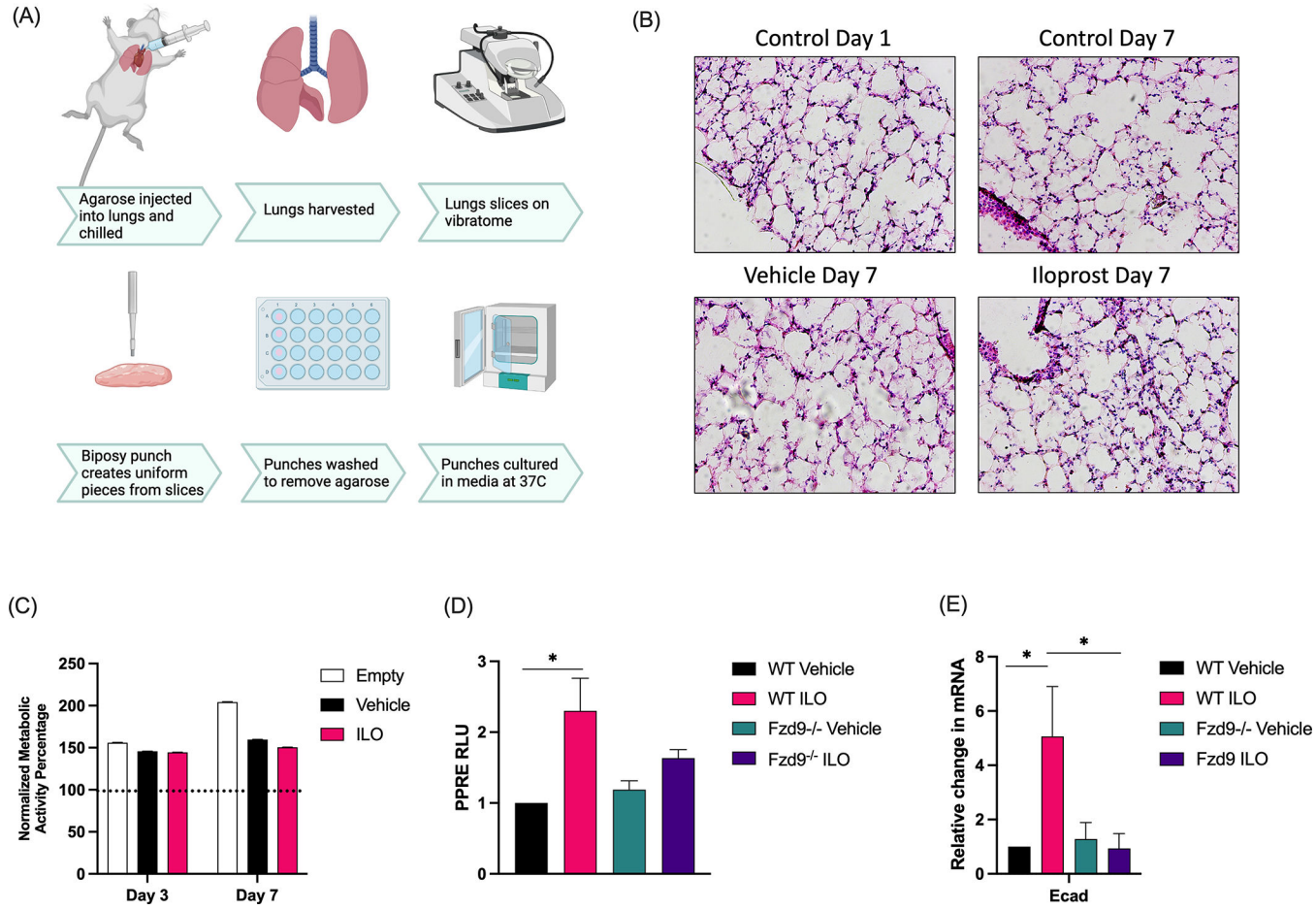

Figure 1. PCLS viability, structure, and signaling is maintained with iloprost treatment.

(A) Schematic of the PCLS generation process. (Diagram created with Biorender.com.) (B) H&E of frozen wild type mouse PCLS at day 1 and day 7 after treatment with Iloprost (3.6μg/ml), vehicle, or empty control. (C) A Presto Blue assay measured viability of wild type mouse PCLS at day 1, 3, and 7 during treatment with vehicle, iloprost (3.6μg/ml), or empty (n=5). Data is shown relative to day 1 (dotted line). (D) PPARγ signaling was measured by PPRE luciferase assay in culture media from PCLS with vehicle or iloprost (3.6ug/ml) at day 6. Data is shown relative to WT control and the assay was conducted in triplicate (n=3). (E) E-cadherin expression in tissue from WT or Fzd9$^{-/-}$ mice with control or iloprost (3.6μg/ml) was measured by qPCR. Assays were conducted in triplicate, data is normalized to RPS18 and shown relative to WT control (n=3). WT, wild type; Fzd9$^{-/-}$. Frizzled 9 knockout; ILO, iloprost. Error bars are SEM. Significance was measured by one-way ANOVA with Tukey post-hoc analysis. *p≤0.05

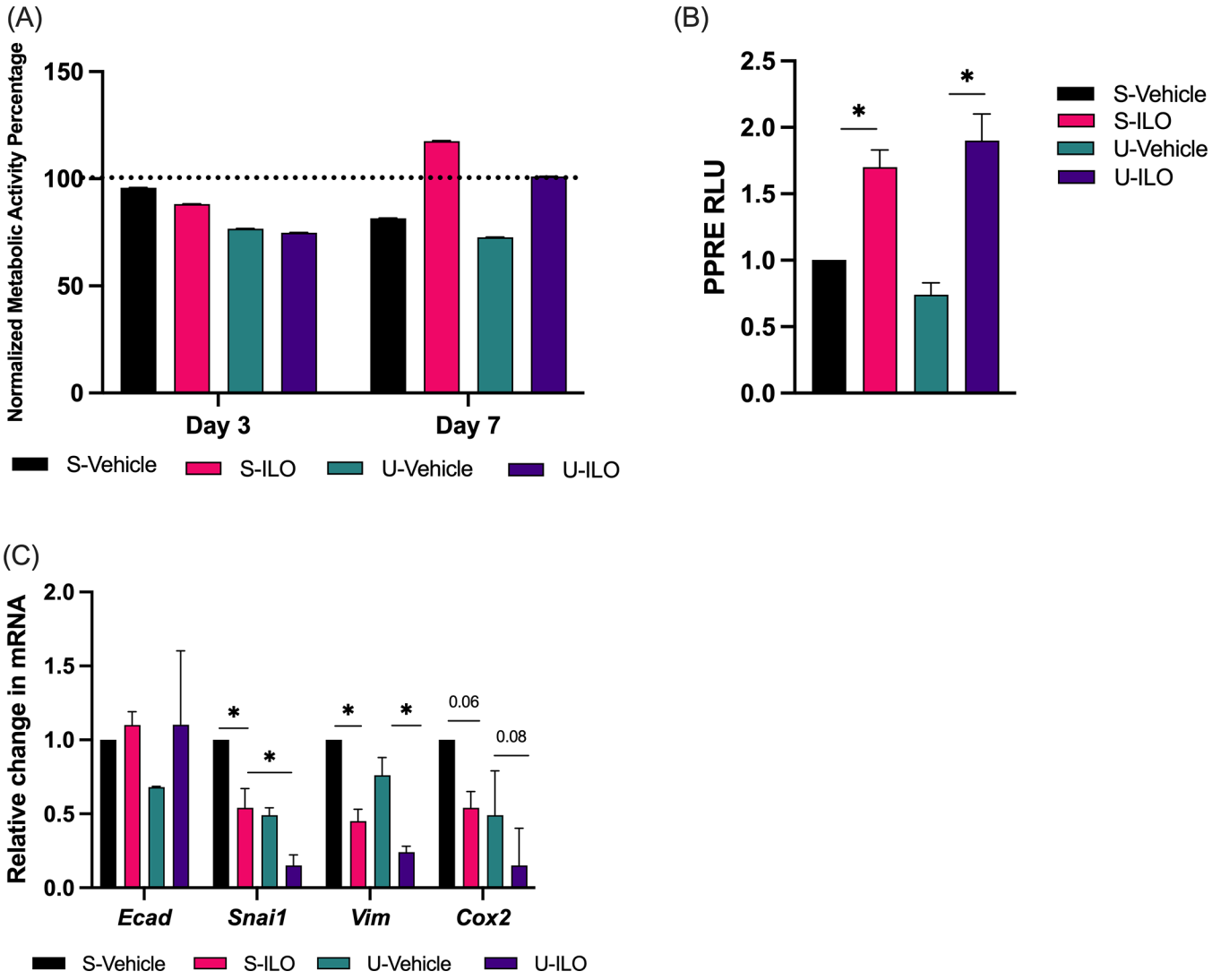

Figure 2. PCLS from *in vivo* urethane treated mice respond to iloprost *ex vivo*.

(A) Viability of PCLS measured by a Presto Blue assay at day 1, 3, and 7 in saline or urethane *in vivo* exposed mice treated with iloprost (3.6ug/ml) or vehicle *ex vivo*. Data is shown relative to day 1 (dotted line) and the assay was conducted in triplicate. (B) PPARγ activity was measured in triplicate at day 3 by PPRE luciferase in PCLS culture media after iloprost (3.6ug/ml) or vehicle *ex vivo*. Data is relative to S-Vehicle. (C) Gene expression was measured by qPCR at day 7 in mice treated with iloprost (3.6μg/ml) or vehicle *ex vivo*. The assays were conducted in triplicate, data are normalized to RPS18 and displayed relative to S-vehicle control. Significance was measured by one-way ANOVA with Tukey's posthoc analysis. *pδ0.05. N=3. S-Vehicle, *in vivo* saline + *ex vivo* vehicle; S-ILO, *in vivo* saline + *ex vivo* iloprost; U-Vehicle, *in vivo* urethane + *ex vivo* vehicle; U-ILO, *in vivo* urethane + *ex vivo* iloprost.

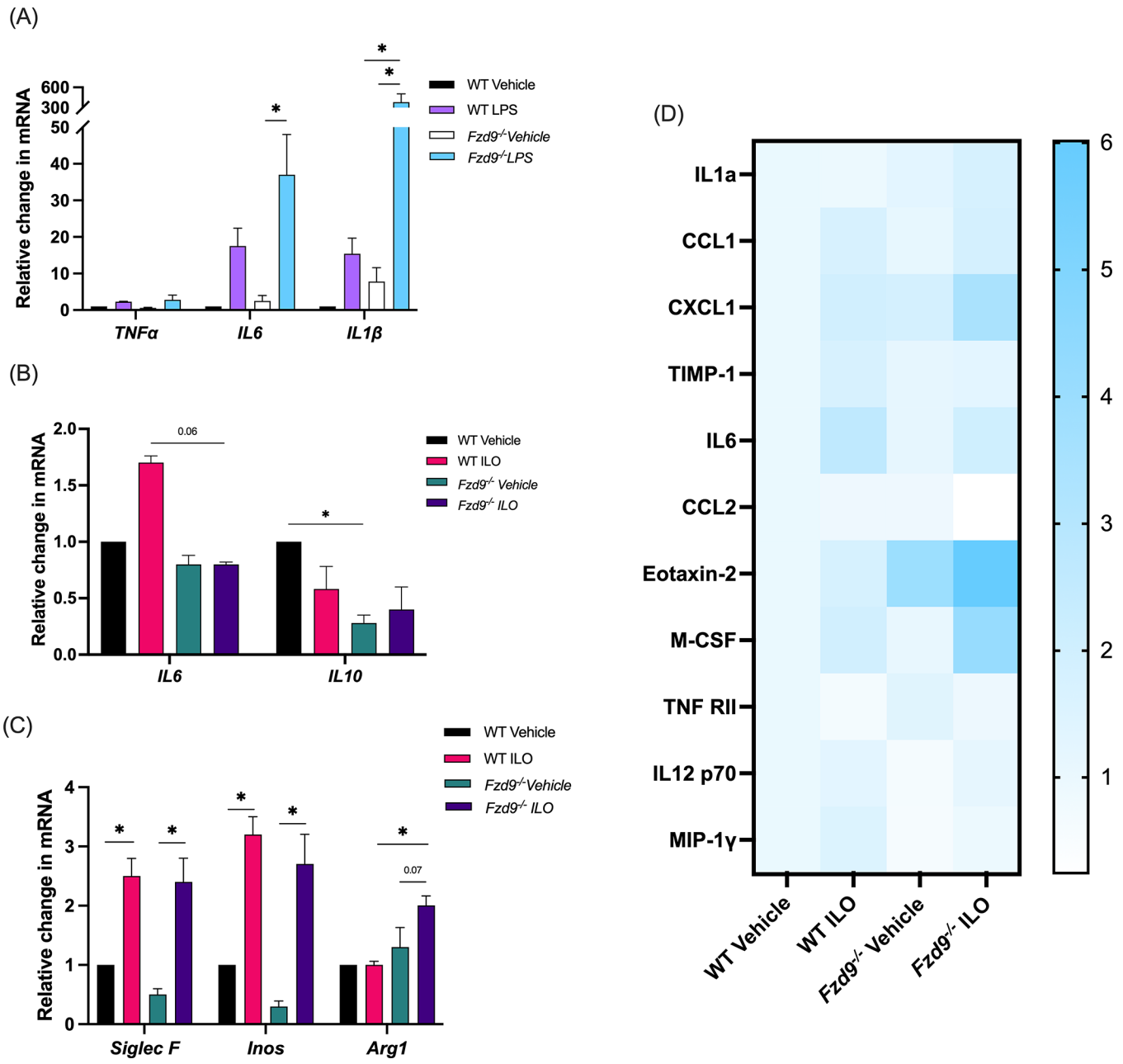

Figure 3. Immune and inflammatory differences are detected in PCLS with iloprost.

(A) WT and Fzd9$^{-/-}$ PCLS were treated with LPS (10ng/ml) for 48 hours and response was measured by qPCR. (B-C) WT and Fzd9$^{-/-}$ PCLS were treated with iloprost (10μM) or vehicle for 7 days and expression of inflammatory markers (B) and macrophage markers (C) was measured by qPCR. All PCR assays were conducted in triplicate, data is normalized to RPS18 and relative to WT Vehicle. (n=3) (D) WT and Fzd9−/− PCLS were treated with iloprost (3.6ug/ml) or vehicle for 7 days. Protein expression was quantified by dot blot. Data is fold change relative to WT Vehicle. (Blot images in Supplementary Figure S1, n=1). Significance was measured by one-way ANOVA with Tukey's post-hoc analysis. *pδ0.05. WT, wild type; ILO, iloprost. *Fzd9*$^{-/-}$, Frizzled 9 knockout.

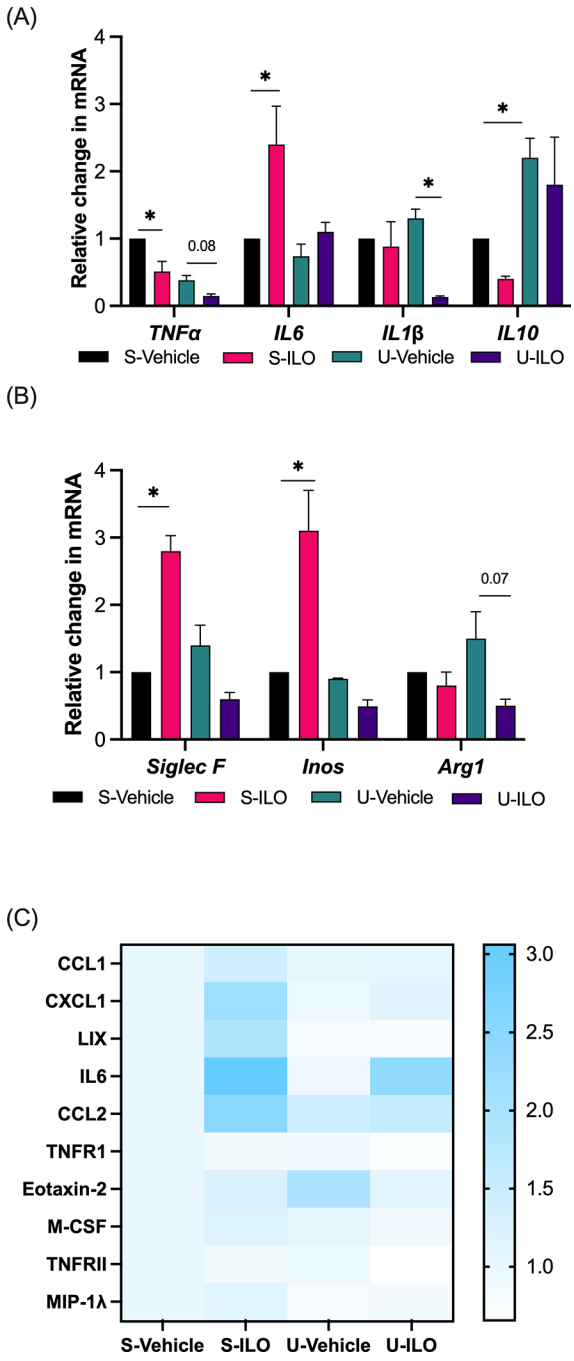

Figure 4. Immune and inflammatory markers in urethane and iloprost exposed PCLS.

Inflammatory (A) and macrophage (B) markers were measured by qPCR at day 7 in urethane or saline *in vivo* exposed mice treated iloprost (3.6μg/ml) or vehicle in PCLS *ex vivo*. Assays were conducted in triplicate, data are normalized to RPS18 and displayed relative to saline-vehicle control (n=3). (C) Expression of cytokines in pooled PCLS culture media was measured by dot blot (Blot images in Supplementary Figure S2, n=1). Significance was measured by one-way ANOVA with Tukey's posthoc analysis. *pδ0.05.

S-Vehicle, *in vivo* saline + *ex vivo* vehicle; S-ILO, *in vivo* saline + *ex vivo* iloprost; U-Vehicle, *in vivo* urethane + *ex vivo* vehicle; U-ILO, *in vivo* urethane + *ex vivo* iloprost.

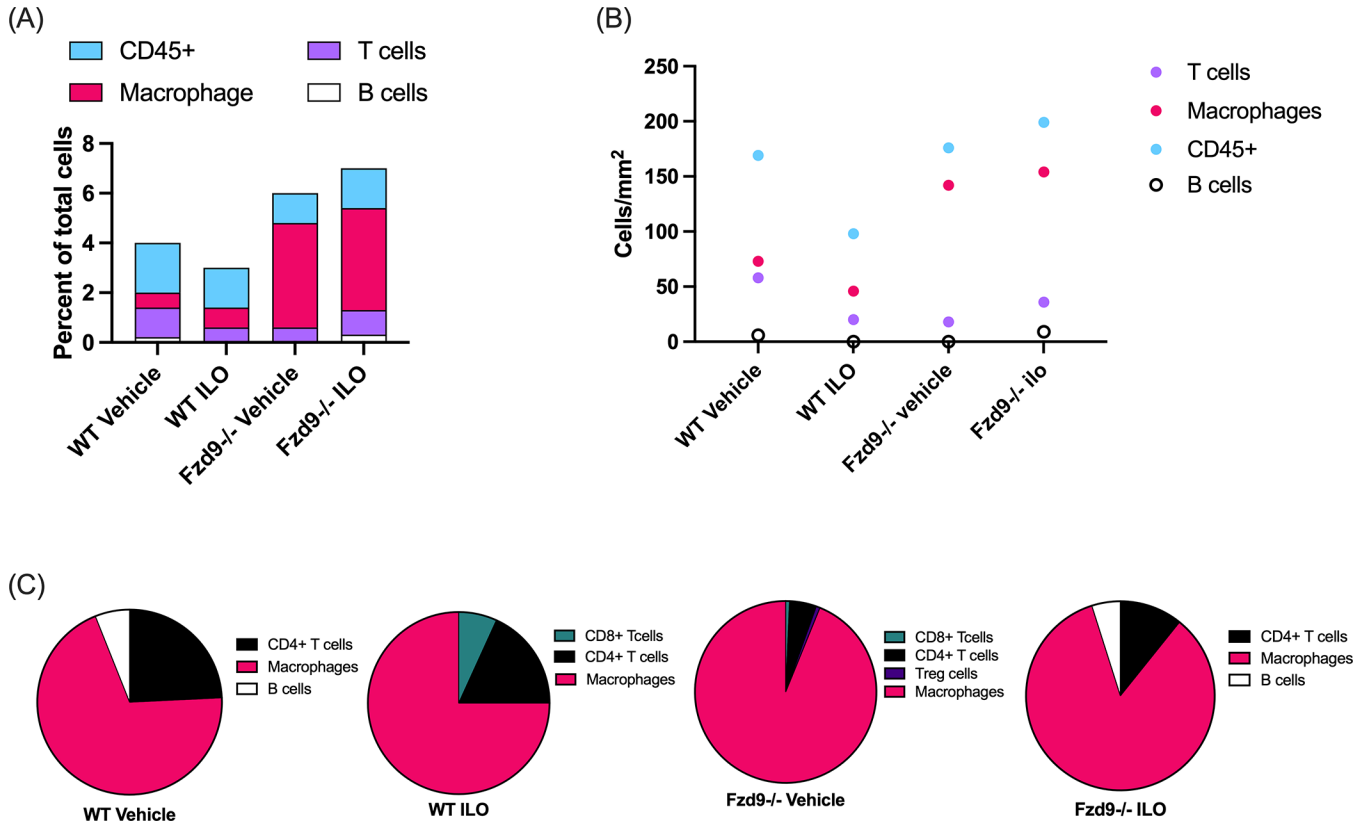

Figure 5. Changes in immune cell markers observed in PCLS with iloprost treatment.

Cell types were characterized by Vectra Polaris assay. (A) Percent of total cells labeled as CD45+, T cells, macrophages, and B cells for each mouse group. (B) Normalized cell density of T cells, macrophages, and B cells. (C) Percent of cell types among CD45+ cells from each mouse group. (n=1) WT, wild type; $Fzd9^{-/-}$, Fzd9 knockout; ILO, iloprost.

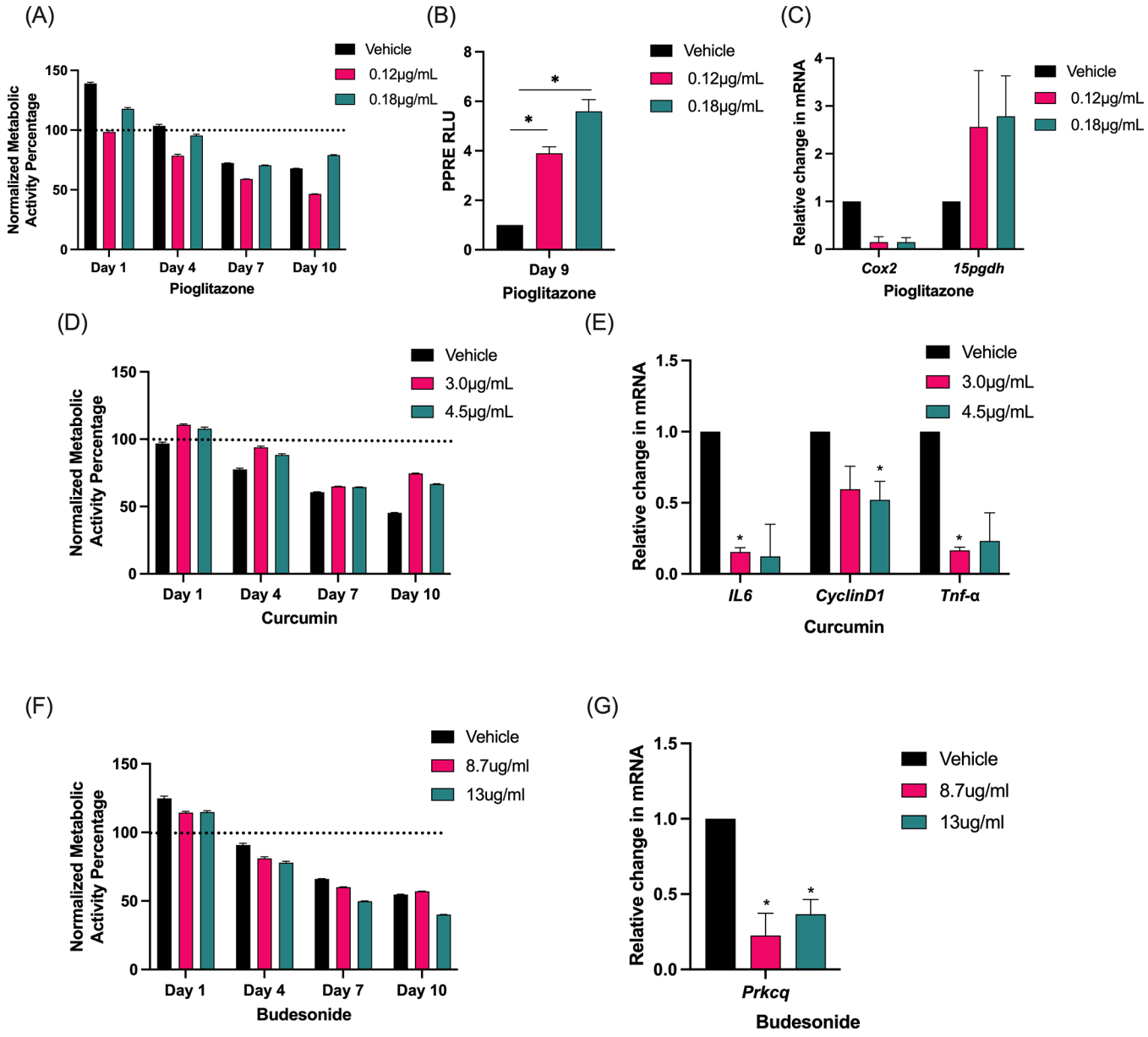

Figure 6. PCLS recapitulates chemoprevention effects.

(A) A Presto Blue assay measured viability during treatment of PCLS with pioglitazone or vehicle control at day 0, 1, 4, 7, and 10. (B) PPRE luciferase activity was measured at day nine in PCLS culture media with pioglitazone or vehicle. The assay was conducted in triplicate and data is shown relative to vehicle. (C) Response to pioglitazone was measured by qPCR at day 10. (D) A Presto Blue assay measured viability during treatment of PCLS with two doses of curcumin or vehicle control at day 0, 1, 4, 7, and 10. (E) Response to curcumin was measured by qPCR. (F) A Presto Blue assay measured viability during treatment of PCLS with two doses of budesonide or vehicle at day 0, 1, 4, 7, and 10. (G) Response to budesonide was measured by qPCR. All presto blue assays were conducted in triplicate and data relative to day zero (dotted line). All qPCR assays were conducted in triplicate, data normalized to RPS18 and shown relative to control. Error bars are SEM.

Significance was measured by one way ANOVA with Tukey's post hoc analysis. n=3 *pδ0.05.